Flinders UNIVERSITY

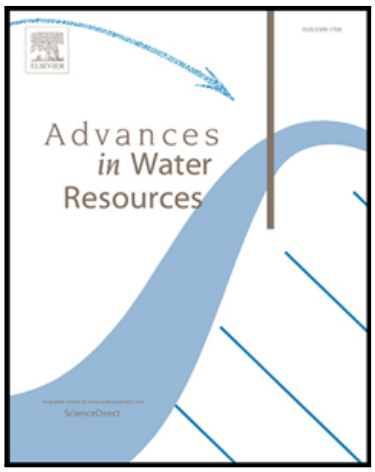

Revisiting analytical solutions for steady interface flow in subsea aquifers: Aquitard salinity effects

Adrian D. Werner , Neville I. Robinson

PII: S0309-1708(17)30906-5
DOI: 10.1016/j.advwatres.2018.01.002
Reference: ADWR 3058

To appear in: *Advances in Water Resources*

Received date: 20 September 2017
Revised date: 3 January 2018
Accepted date: 3 January 2018

Please cite this article as: Adrian D. Werner , Neville I. Robinson , Revisiting analytical solutions for steady interface flow in subsea aquifers: Aquitard salinity effects, *Advances in Water Resources* (2018), doi: 10.1016/j.advwatres.2018.01.002

Highlights:

- Subsea fresh groundwater analytical solution revised to include aquitard salinity
- Comparison to numerical modelling demonstrates aquitard salinity effects
- Solution produces improved discharge to the sea and interface tip location
- Further work is required to assess dispersion effects on interface distribution

Revisiting analytical solutions for steady interface flow in subsea aquifers: Aquitard salinity effects

Adrian D. Werner*[1,2] and Neville I. Robinson[1]

[1]College of Science and Engineering, Flinders University, GPO Box 2100, Adelaide, SA 5001, Australia.

[2]National Centre for Groundwater Research and Training, Flinders University, GPO Box 2100, Adelaide, SA 5001, Australia.

*Corresponding author

Email addresses:

Adrian Werner: adrian.werner@flinders.edu.au

Neville Robinson: gleammx@gmail.com

Submitted to *Advances in Water Resources* on 20th September 2017

Abstract

Existing analytical solutions for the distribution of fresh groundwater in subsea aquifers presume that the overlying offshore aquitard, represented implicitly, contains seawater. Here, we consider the case where offshore fresh groundwater is the result of freshwater discharge from onshore aquifers, and neglect paleo-freshwater sources. A recent numerical modelling investigation, involving explicit simulation of the offshore aquitard, demonstrates that offshore aquitards more likely contain freshwater in areas of upward freshwater leakage to the sea. We integrate this finding into the existing analytical solutions by providing an alternative formulation for steady interface flow in subsea aquifers, whereby the salinity in the offshore aquitard can be chosen. The new solution, taking the aquitard salinity as that of freshwater, provides a closer match to numerical modelling results in which the aquitard is represented explicitly.

1. Introduction

Freshwater is known to occur in a multitude of offshore aquifers around the globe (Post et al., 2013). Fresh groundwater in offshore aquifers may derive from the continental discharge that occurs under present-day conditions, and/or may have been emplaced during the low sea levels of glacial maxima during the Pleistocene epoch (Cohen et al., 2010). Methods for the rapid estimation of offshore freshwater extent attributable to continental discharge include the analytical solutions of Edelman (1972), Kooi and Groen (2001), and Bakker (2006). Bakker et al. (2017) provide an extension to Bakker's (2006) solution by modifying the landward boundary condition and correcting an error in the graphical representation of the methodology. These methods have proven to be beneficial

for the initial investigation of offshore freshwater in subsea aquifers, including their potential to supplement onshore groundwater pumping. For example, Bakker (2006) found that the hydrogeological conditions near the Georgia-Florida border (USA) are sufficient to have created an extensive offshore freshwater body in continental shelf aquifers.

The cross-sectional conceptual model for offshore freshwater adopted by Bakker (2006) and others is illustrated in Figure 1, showing an onshore confined aquifer connected to an offshore leaky aquifer. The dual aquifer system in the onshore setting is simplified to an onshore confined aquifer to avoid the mathematical challenge of resolving connected upper and lower aquifers.

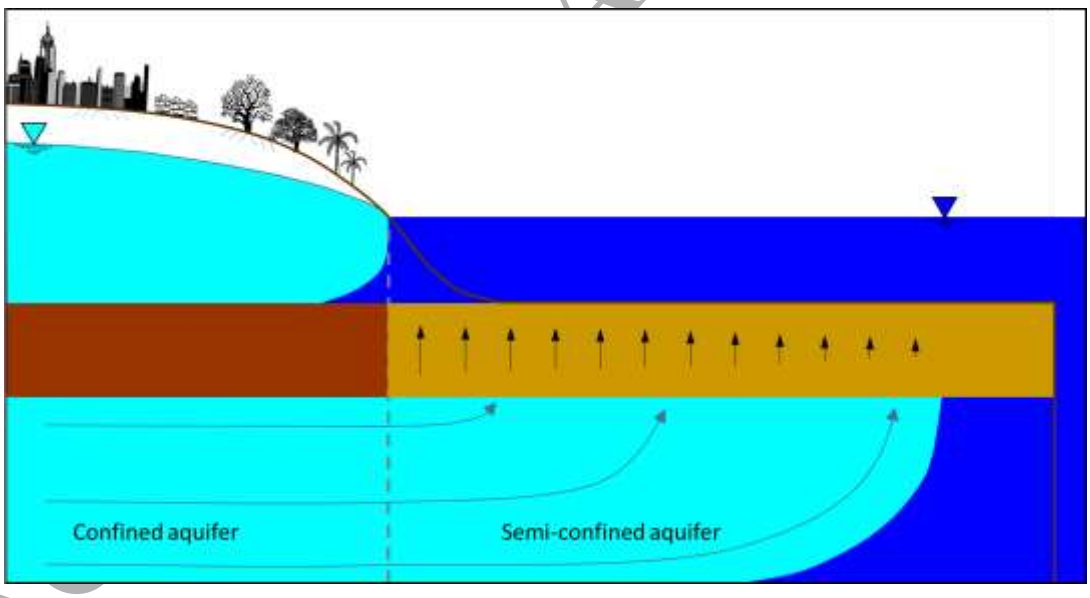

Figure 1. Conceptual model of offshore fresh groundwater (light blue) created by an onshore confined aquifer discharging to a semi-confined offshore aquifer. Dark blue regions are seawater.

The analytical solutions provided by Bakker (2006) and Bakker et al. (2017) (referred to collectively as Bakker's solutions in the remainder) require an assumption for the salinity in offshore aquitards, which overly offshore aquifers and inhibit the freshwater-seawater mixing that would otherwise degrade the subsea freshwater. They presume that offshore aquitards contain seawater, even where they host upward freshwater leakage to the sea from underling aquifers. In a concurrent numerical modelling investigation, Solórzano-Rivas and Werner (2017) show that offshore aquitards are more likely to contain freshwater where upward freshwater leakage occurs. They also provide a methodology for correctly simulating offshore aquitards using the implicit approach of the popular SEAWAT code (Langevin et al., 2008). Solórzano-Rivas and Werner (2017) conclude that Bakker's solutions over-predict the offshore extent of freshwater by a factor of approximately two due to the assumption that offshore aquitards contain seawater. They recommend that a revision to Bakker's solutions is required, whereby offshore aquitards are presumed to contain freshwater in areas of upward leakage to the sea.

The aim of this research is to provide a sharp-interface mathematical model under Dupuit assumptions for the offshore aquitard containing water with salinity ranging from that of freshwater to seawater, thereby incorporating Bakker's solutions as a special case. We anticipate that this will overcome the discrepancies between analytically derived interface locations and those obtained from numerical simulation, such as those of Solórzano-Rivas and Werner (2017). The quality of the revised analytical model is demonstrated by comparing with results from SEAWAT.

2. Mathematical model of semi-confined interface flow

The aim of the following mathematical development is to determine and calculate a head-distance relationship given a confined aquifer onshore and its finite-length extension below the sea surface as a semi-confined aquifer, i.e., overlain by a leaking aquitard. The notation used by Bakker (2006) is largely followed. The offshore part of the problem is shown schematically in Fig. 2.

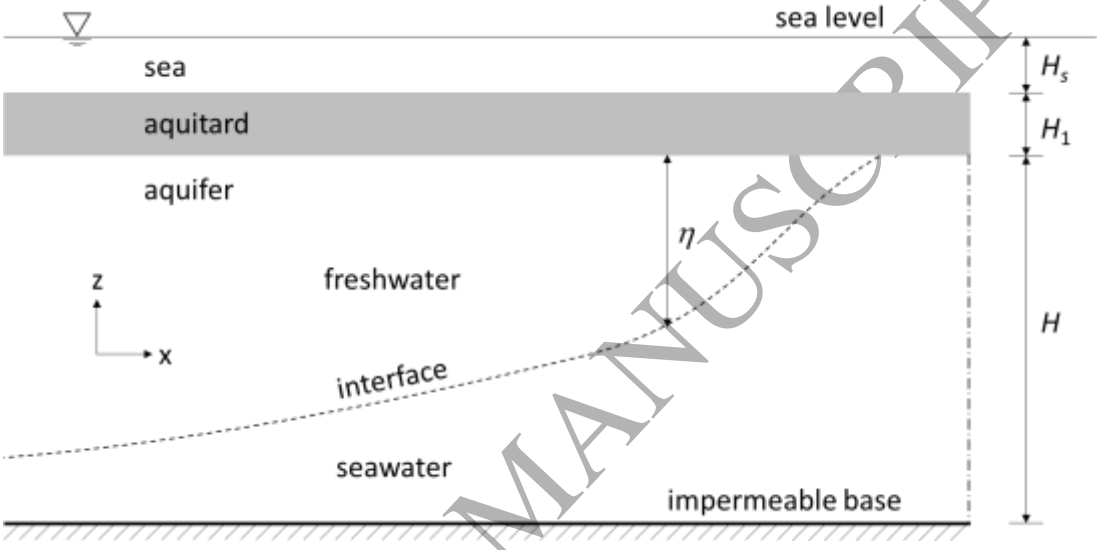

Figure 2. Conceptual model of the semi-confined offshore aquifer (modified from Bakker, 2006).

The freshwater head, h_1, of the sea at the top of the aquitard, is given by

$$h_1 = z_s + \nu_s H_s \tag{1}$$

where, as shown in Fig. 2, H_s is the height of the sea surface above the aquitard, and z_s is the elevation of the sea. The datum for z_s is arbitrary but commonly taken as the impermeable base of the aquifer or sea level. The dimensionless density difference between seawater and freshwater, ν_s, is given by

$$\nu_s = \left(\rho_s - \rho_f\right)/\rho_f \tag{2}$$

with ρ_f and ρ_s the respective densities for freshwater and seawater.

The use of Darcy's Law to calculate flow across the offshore aquitard to the ocean in regions where the aquifer contains freshwater requires presumption of the aquitard salinity. That is

$$q_z = \frac{K_v}{H_1}\left(h - h_t - \frac{\left(\rho_a - \rho_f\right)}{\rho_f} \right) \tag{3}$$

h is the head in the freshwater region of the aquifer, K_v is the hydraulic conductivity of the leaking aquitard, and ρ_a is the density of the aquitard fluid. Bakker's (2006) assumption of seawater in the aquitard leads to $\rho_a = \rho_s$, whereas if the aquitard contains freshwater, $\rho_a = \rho_f$ and the buoyancy term of Eq. (3) disappears. We introduce the factor α, whereby $\alpha = 0$ represents the seawater assumption of Bakker (2006) and Bakker et al. (2017), $\alpha = 1$ is the freshwater assumption, and $0 < \alpha < 1$ is mixed seawater and freshwater. Rewriting Eq. (3) in terms of v_s and α

$$q_z = K_v\left(\frac{\left(h - h_1\right)}{H_1} - \left(1 - \alpha\right)v_s \right) \tag{4}$$

where H_1 is the aquitard thickness, as shown in Figure 2. Note that we assume that the aquitard overlying the fresh part of the offshore aquifer contains only one salinity type, i.e., there is no salinity spatial variability.

Bakker (2006) writes Eq. (4) in terms of the freshwater head, h_s, of a column of static seawater at the level of the horizontal top of the aquifer

$$h_s = z_s + v_s\left(H_s + H_1\right) \tag{5}$$

h_s is also equal to the head at the top of the aquifer (h_1) plus the buoyancy force caused by seawater in the aquitard, and is convenient to adopt because freshwater occurs in the

aquifer only where $h > h_s$ (Werner, 2017). Combining Eqs. (5) and (3), and letting $\rho_a = \rho_s$ (i.e., presuming the aquitard contains seawater) produces (Bakker, 2006)

$$q_z = \frac{K_v}{H_1}(h - h_s) \tag{6}$$

The thickness, η, of the freshwater zone (see Figure 2) is approximated by the Ghyben-Herzberg formula (e.g. Bear, 1979)

$$\eta = (h - h_s)/v_s \tag{7}$$

Assuming Darcy's law and the Dupuit approximation, the vertically integrated freshwater discharge, Q_x, at distance x (of arbitrary origin; see Fig. 2) is defined by

$$Q_x = -K\eta\frac{dh}{dx} \tag{8}$$

with K the constant hydraulic conductivity of the aquifer. Flow continuity requires

$$-\frac{dQ_x}{dx} = \frac{d}{dx}\left(K\eta\frac{dh}{dx}\right) = q_z \tag{9}$$

Eq. (4) becomes, on using Eqs. (1) and (5) and introducing $c = H_1/K_v$,

$$q_z = \frac{K_v(h - h_1 + \alpha H_1 v_s)}{H_1} - K_v v_s = \frac{(h - h_s + \alpha H_1 v_s)}{c} \tag{10}$$

Now, using Eq. (7) for η and Eq. (10) for q_z, the continuity Eq. (9) becomes

$$\frac{d}{dx}\left[\frac{K(h - h_s)}{v_s}\frac{dh}{dx}\right] = \frac{(h - h_s + \alpha H_1 v_s)}{c} \tag{11}$$

Non-dimensional variables ϕ, ζ and ξ are now defined by

$$\phi = \frac{(h - h_s)}{v_s H},\ \zeta = 1 - \phi,\ \xi = \frac{x}{l_f} \tag{12}$$

Here, ζ is the vertical dimensionless distance from aquifer base to interface, H is the depth of the base below the aquitard (as in Fig. 2), and the leakage factor is defined by $l_f = \sqrt{kHc}$.

Eq. (11) now becomes

$$\frac{d}{d\xi}\left(\phi \frac{d\phi}{d\xi}\right) = \phi + \alpha H_1^* \tag{13}$$

with $H_1^* = H_1/H$. The quantity αH_1^* is to be considered as a single quantity, because neither α nor H appear separately in the analysis. The introduction of the quantity αH_1^* and its ramifications in the ensuing analysis is the generalisation of Bakker's original model.

Following the procedure used by Bakker (2006) and Sikkema and van Dam (1982), Eq. (13) is solved by first multiplying throughout by ϕ:

$$\phi \frac{d}{d\xi}\left(\phi \frac{d\phi}{d\xi}\right) = \phi \frac{d}{d\phi}\left(\phi \frac{d\phi}{d\xi}\right)\frac{d\phi}{d\xi} = \frac{1}{2}\frac{d}{d\phi}\left[\phi \frac{d\phi}{d\xi}\right]^2 = \phi^2 + \alpha H_1^* \phi \tag{14}$$

Now integrate to obtain

$$\left(\phi \frac{d\phi}{d\xi}\right)^2 = \frac{2}{3}\left(\phi^3 + \frac{3}{2}\alpha H_1^* \phi^2 + a^3\right) \tag{15}$$

with *a* a constant to be determined by boundary conditions. At this stage, it is convenient to introduce a dimensionless discharge, γ_u, by

$$\gamma_u = \frac{Q_x l_f}{KH^2 \nu_s} = -\phi \frac{d\phi}{d\xi} \tag{16}$$

The particular value of γ_u at the shoreline where $Q_x = Q_0$ (and $\phi = \phi_0$) is denoted by γ_0:

$$\gamma_0 = \mu = \frac{Q_0 l_f}{KH^2 \nu_s} \tag{17}$$

where μ is one of the three key parameters, the others being αH_1^* and $\lambda_s = L_s / l_f$. The length of the aquitard from the shoreline is denoted by L_s.

Taking the square root of both sides of Eq. (15) and using the negative root of the right side to give a positive γ_u:

$$\gamma_u = \sqrt{\frac{2}{3}} \sqrt{\phi^3 + 3/2\, \alpha H_1^* \phi^2 + a^3} \tag{18}$$

From Eq. (15), a further integration gives

$$\xi = -\sqrt{\frac{3}{2}} \int \frac{\phi}{\sqrt{\phi^3 + 3/2\, \alpha H_1^* \phi^2 + \alpha^3}}\, d\phi + b \tag{19}$$

where *b* is another constant to be determined by boundary conditions.

Bakker (2006) defines four cases of interface problems arising from the above theory. These are defined based on whether the toe (where the interface meets the impermeable aquifer base) is onshore (Cases I and III) or offshore (Cases II and IV), and whether the

tip (where the interface meets the base of the offshore aquitard) is landward of the most seaward boundary (Cases I and II) or the tip reaches the offshore limit (Cases III and IV).

From this point, the analysis divides into two sections depending on whether $a = 0$, defining Cases I and II, or $a \neq 0$, defining Cases III and IV. Another division, introduced for simplicity of analysis, is to consider different origins for variable ξ depending on the location of the toe. For Cases I and III, with the toe onshore, set $\xi = \xi_1$ for Case I and $\xi = \xi_3$ for Case III, with $\xi_1 = \xi_3$ and both variables originating at the shoreline. Although the introduction of the two coordinates having the same origins is mathematically redundant, it is useful to have them when focussing on the particular cases. Similarly with the toe offshore (Cases II and IV) and the corresponding origin at the toe, $\xi = \xi_2$ for Case II, $\xi = \xi_4$ for Case IV, and $\xi_2 = \xi_4$. Figs. 3a, 3b, 3c, 3d show typical curves of the head and interface for some selected parameter combinations, each falling into one of the four cases. The numerical values used for constructing these curves are given in Table 1.

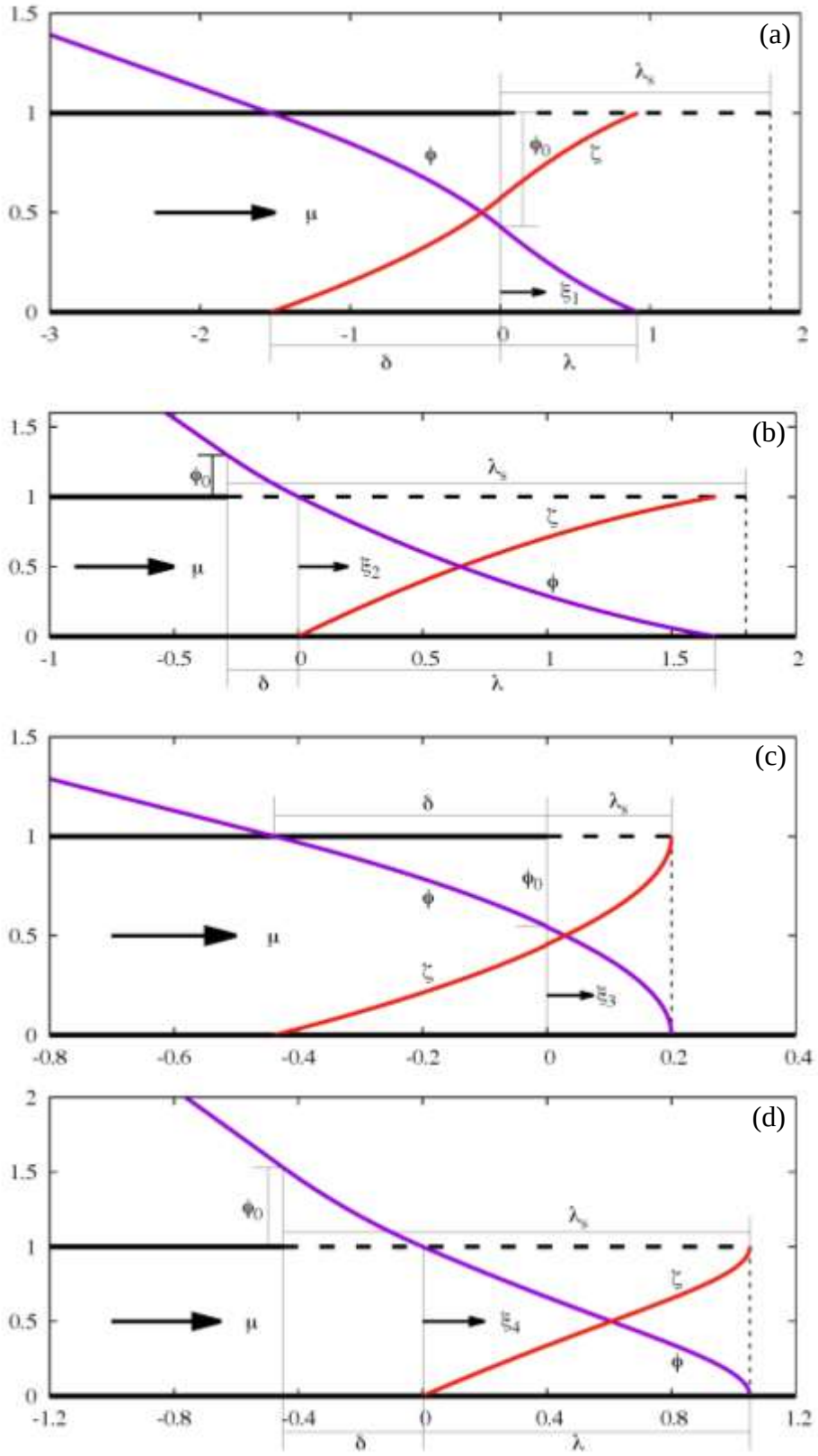

Figure 3. Typical case diagrams for non-dimensional lengths, heads and interface: (a) Case I, (b) Case II, (c) Case III, and (d) Case IV. The axes are dimensionless, as defined

by Eqs. (12). The solid horizontal lines represent no-flow boundaries, while the dashed horizontal line represents the base of the leaking aquitard.

Table 1. Parameter values used in Figures 3a, 3b, 3c, 3d. Parameters are defined in the text that follows.

Figure (Case)	μ	λ	λ_s	δ	ϕ_0	a	β
3a (I)	0.2669	0.9159	$> \lambda$	1.5729	0.4294	0	-
3b (II)	1.2290	1.6781	$> \lambda + \delta$	0.2849	1.2978	0	-
3c (III)	0.8	0.2	0.2	0.4383	0.5465	0.9094	1.0581
3d (IV)	1.5	1.0522	1.5	0.4478	1.5283	0.3973	1.1430

The quantities ϕ_0 and δ represent, respectively, the head at the shoreline and the distance of the toe from its origin. λ is defined in the same way as λ_s, namely $\lambda = L/l_f$, where L is the length from origin to tip. In Case I, $\lambda < \lambda_s$; in Case II, $\lambda + \delta < \lambda_s$; in Case III, $\lambda = \lambda_s$; and in Case IV, $\lambda + \delta = \lambda_s$.

Fig. 4 illustrates the division of the cases into four zones on the basis of μ and λ_s. The boundaries of the zones are designated: Γ_{12}, between Cases I and II; Γ_{13}, between Cases I and III; Γ_{24}, between Cases II and IV; and Γ_{34}, between Cases III and IV. A number of individual points are shown on the diagram, labelled M_1 to M_6, F_3, F_4 and P_4. These points are used in various parts of the analysis that follows. M_4, M_6, F_3 and F_4 coincide with the parameter sets (see Table 1) used to create Figures 3a, 3b, 3c and 3d, respectively. Point P_4 is a quadruple point where all four boundaries meet with coincidence of offshore tips and shoreline toes. This diagram is essentially one defining zones for Cases III and IV with the horizontal axis as λ_s. Classes I and II are defined solely by the value of μ, because their tip values are less than the given non-dimensional

λ_s. The areas designated as I and II in the figure have all parameter values constant within them. The points M_1 to M_6 are located on the joined boundaries $\Gamma_{13} - \Gamma_{24}$ to indicate their shore to tip values, less than those at the aquitard seaward end.

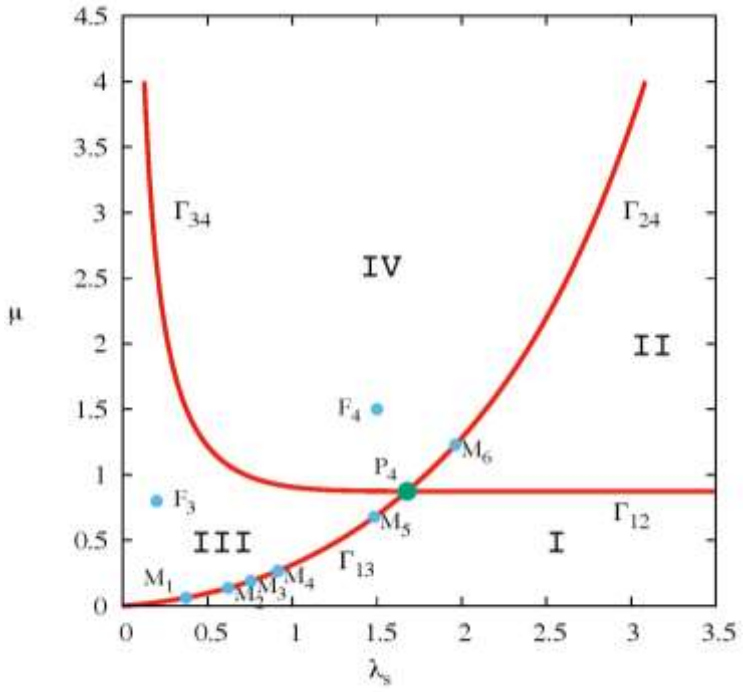

Figure 4. Zones for Cases 1 to IV. $\alpha H_1^* = 0.1$.

Summary of head equations from toe to tip

Details of the derivations of the following equations are given in the Appendix, including explicit expressions for ϕ_0 and $\delta = d/l_f$ occurring below, with *d* the distance from toe to shoreline. For all four cases, $\phi = 1$ ($\zeta = 0$) at the toe and $\phi = 0$ ($\zeta = 1$) at the tip. The final expressions are:

Case I:

From shore to toe: $$\phi^2 = -2\mu\xi_1 + \phi_0^2, \quad -\delta \le \xi_1 \le 0 \tag{20}$$

From shore to tip: $$\phi = \frac{1}{6}\left[(\xi_1 - \lambda)\left(\xi_1 - \lambda - 6\sqrt{\alpha H_1^*}\right)\right], \quad 0 \le \xi_1 \le \lambda \tag{21}$$

Case II:

Beyond the toe, Eq. (21) is also applicable in this case, but with ξ_1 replaced by ξ_2:

$$\phi = \frac{1}{6}\left[(\xi_2 - \lambda)\left(\xi_2 - \lambda - 6\sqrt{\alpha H_1^*}\right)\right], \quad 0 \le \xi_2 \le \lambda \tag{22}$$

Between toe and shoreline:

$$\phi = \frac{1}{2}\left(1 - \gamma_0 + \alpha H_1^*\right)e^{\xi_2} + \frac{1}{2}\left(1 + \gamma_0 + \alpha H_1^*\right)e^{-\xi_2} - \alpha H_1^*, \quad -\delta \le \xi_2 \le 0 \tag{23}$$

with $\gamma_0 = \sqrt{2/3 + \alpha H_1^*}$.

Case III:

The expression from shoreline to tip for ϕ is implicit, involving cubic equations and elliptic integrals:

$$\xi_3 = \sqrt{\frac{3\beta\alpha}{2}}\left[f(\phi, a, \beta) - f(0, a, \beta)\right] + \lambda_s, \quad 0 \le \xi_3 \le \lambda_s \tag{24}$$

and $\beta = p/a$ where ($-p$) is the dominant and real zero of $y^3 + 3/2\,\alpha H_1^* y^2 + a^3$, and

$$f(\phi, \alpha, \beta) = \left(\frac{1}{\sqrt{g}} - \sqrt{g}\right)F(\theta, \kappa) + 2\sqrt{g}\,E(\theta, \kappa) - 2\sqrt{g}\,\frac{\sin\theta\sqrt{1 - \kappa^2\sin^2\theta}}{1 + \cos\theta} \tag{25}$$

$F(\theta, \kappa)$ and $E(\theta, \kappa)$ are incomplete elliptic integrals of the first and second kinds (e.g. Byrd and Friedman, 1971), respectively, and

$$g = \sqrt{1 + 2/\beta^3}\,, \quad \kappa = \sqrt{\left(1 + 1/\left(2\beta^3\right) + g\right)/(2g)}\,, \quad \theta = \cos^{-1}\left[\frac{g - 1 - \phi/(\beta\alpha)}{g + 1 + \phi/(\beta\alpha)}\right] \tag{26}$$

The constant *a* is determined from boundary conditions at the shoreline where $\phi = \phi_0$

From shoreline to tip, the same expression as Case I (i.e., Eq. (20)) holds and $\xi_1 = \xi_3$:

$$\phi^2 = -2\mu\xi_3 + \phi_0^2, \quad -\delta \le \xi_3 \le 0 \tag{27}$$

Case IV:

From toe to tip, the same form of equation as in Eq. (24) holds, but with coordinate ξ_4:

$$\xi_4 = \sqrt{\frac{3\beta\alpha}{2}}\left[f(\phi, a, \beta) - f(0, a, \beta)\right] + \lambda_s, \quad 0 \le \xi_4 \le \lambda_s \tag{28}$$

with constant *a* now determined from conditions at the tip, where $\phi = 1$ and $\xi_4 = \lambda = \lambda_s - \delta$.

From toe to shoreline:

$$\phi = \left(1 + \alpha H_1^*\right)\frac{\cosh(\delta + \xi_4)}{\cosh\delta} - \mu\frac{\sinh\xi_4}{\cosh\delta} - \alpha H_1^*, \quad -\delta \le \xi_4 \le 0 \tag{29}$$

Inland head equations

The equation for inland head in the confined aquifer beyond the toe in Cases I and III, depicted in Figs. 3a and 3b is

$$\phi = -\mu\left(\xi_{1,3} + \delta\right) + 1 \tag{30}$$

whereas inland from the shoreline in Cases II and IV, shown in Figs. 3c and 3d, it is

$$\phi = -\mu\left(\xi_{2,4} + \delta\right) + \phi_0 \tag{31}$$

Eqs. (30) and (31) are linear in ϕ and are used when one or two of the parameters μ, λ_s and αH_1^* are not known. For one unknown, values of head and distance at a single point

are required, the most likely case being to find μ given λ_s and αH_1^*. For two parameters unknown, values at two inland points are required. A third point will not produce any new information for finding three unknowns because of the linear equations for ϕ.

Mathematical details of zone boundaries

The specific expressions defining the borders between the regions for the different cases with parameters subscripted by *t* (for transition) are defined by:

Border between Cases 1 and 2 (Γ_{12}):

$$\mu_t = \sqrt{2/3 + \alpha H_1^*}, \quad \text{with } \lambda_{st} = L_{st}/l_f \tag{32}$$

Border between Cases 1 and 3 (Γ_{13}):

$$\lambda_{st} = \sqrt{6\phi_0 + 9\alpha H_1^*} - 3\sqrt{\alpha H_1^*} \tag{33}$$

where ϕ_0 in terms of μ is the real solution of the cubic equation

$$\phi_0^3 + 3/2\,\alpha H_1^* \phi_0^2 - 3/2\,\mu_t^2 = 0 \tag{34}$$

Border between Cases 2 and 4 (Γ_{24}):

$$\lambda_{st} = \sqrt{6 + 9\alpha H_1^*} - 3\sqrt{\alpha H_1^*} + \log\left[\frac{\mu + \sqrt{\mu^2 + \left(1 - \gamma_0 + \alpha H_1^*\right)\left(1 + \gamma_0 + \alpha H_1^*\right)}}{\left(1 + \gamma_0 + \alpha H_1^*\right)}\right] \tag{35}$$

with $\gamma_0 = \sqrt{2/3 + \alpha H_1^*}$.

Border between Cases 3 and 4 (Γ_{34}):

$$\sqrt{\frac{3\beta a}{2}}\left[f\left(1, a_t, \beta\right) - f\left(0, a_t, \beta\right)\right] + \lambda_{st} = 0, \text{ with } a_t = \left[3/2\left(\mu_t^2 - \alpha H_1^*\right) - 1\right]^{1/3} \tag{36}$$

The coordinates of the quadruple point P_4 are

$$(\lambda_{s4}, \mu_4) = \left(\left(\sqrt{6+9\alpha H_1^*} - 3\sqrt{\alpha H_1^*}\right), \sqrt{2/3+\alpha H_1^*}\right) \tag{37}$$

3. Numerical details

Iterative procedures are required in calculating $a \neq 0$ involved in expressions containing elliptic integrals. Bakker (2006) chose the robust, but slowly converging method of bisection. This works well because the behaviour of a is monotonic in both μ and λ_s, and $a > 0$. We adopt the more rapid Muller-Frank method (Muller, 1956; Frank, 1958; Matthews and Fink, 2004). Neither method requires function derivatives as opposed to Newton's method. However, computational speed is not an issue here with either method. For example, a grid of 400 x 400 point values for ϕ_0, δ and a used in constructing the contours of Figs. 5a, 5b and 5c (with $\alpha H_1^* = 0.1$) needed a few seconds on a personal computer for the bisection method and approximately a sixth of that for the Muller-Frank method. All programming was done in FORTRAN using available software for computing incomplete elliptic integrals (Carlson and Notis, 1981).

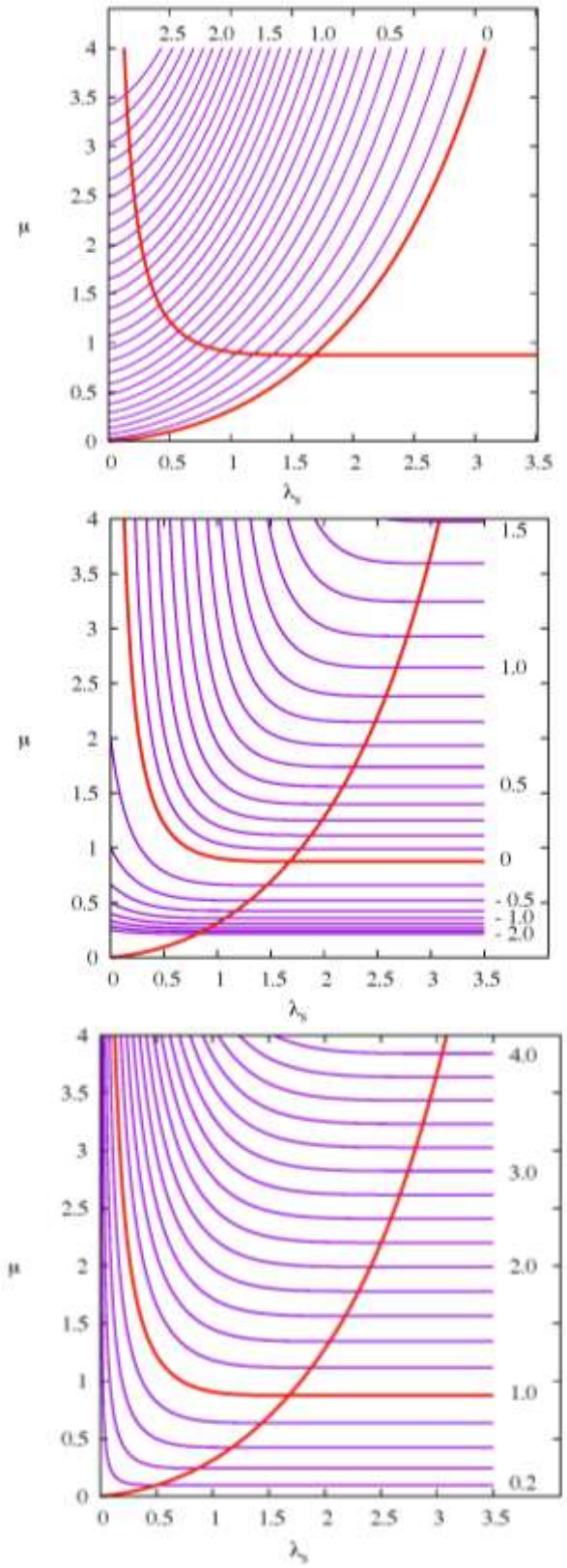

Figure 5. Contour plots (with $\alpha H_1^* = 0.1$) of the following parameters: (a) a (0 to 2.6 in steps of 0.1); (b) δ (-2 to 0 in steps of 0.25, and then 0 to 1.5 in steps of 0.1); (c) ϕ_0 (0.2 to 4 in steps of 0.2).

The contour plots of Fig. 5 are provided to show the behaviours of the quantities ϕ_0 and δ, necessary for describing the head-distance relationships as exemplified in Figs. 3a, 3b, 3c, and 3d; and a, the mathematical constant underpinning the calculations of these two quantities. Superimposed on each of these contour maps are the zonal boundaries of Fig. 4. In Fig. 5a, the boundary Γ_{13} joined with Γ_{24} defines the line $a = 0$. In Fig. 5b, when the toe coincides with the shoreline, the boundary Γ_{12} joined with Γ_{34} defines a line where $\delta = 0$. The negative values of δ correspond to the shoreline to inland toe distances for Cases I and III. The same joining of boundaries also defines where $\phi_0 (= \phi) = 1$ as shown in the contours for ϕ_0 of Fig. 5c. All three contour maps show the expected continuity of values across zonal boundaries and the constancy of values for constant μ outside the joined boundaries $\Gamma_{13} - \Gamma_{24}$ (as shown on Fig. 4).

A contour map of β produces similar contour shapes to those of Fig. 5a. However, it is more instructive to consider variations in λ_s at constant μ and plot values of a, β and βa. This is done for $\mu = 4$ and shown in Fig. 6 with λ_s covering the complete ranges of Cases III and IV. The interesting results are that as $\lambda_s \to \Gamma_{24}$, $a \to 0$, $\beta \to \infty$ but $\beta a \to 3/2\,\alpha H_1^*$ for all αH_1^*, which in this case is 0.15. Other cross sections show the same form of curves and the same limiting values. The infinite value of β does not cause numerical problems because it only occurs separately from βa as $1/\beta$ in Eq. (26).

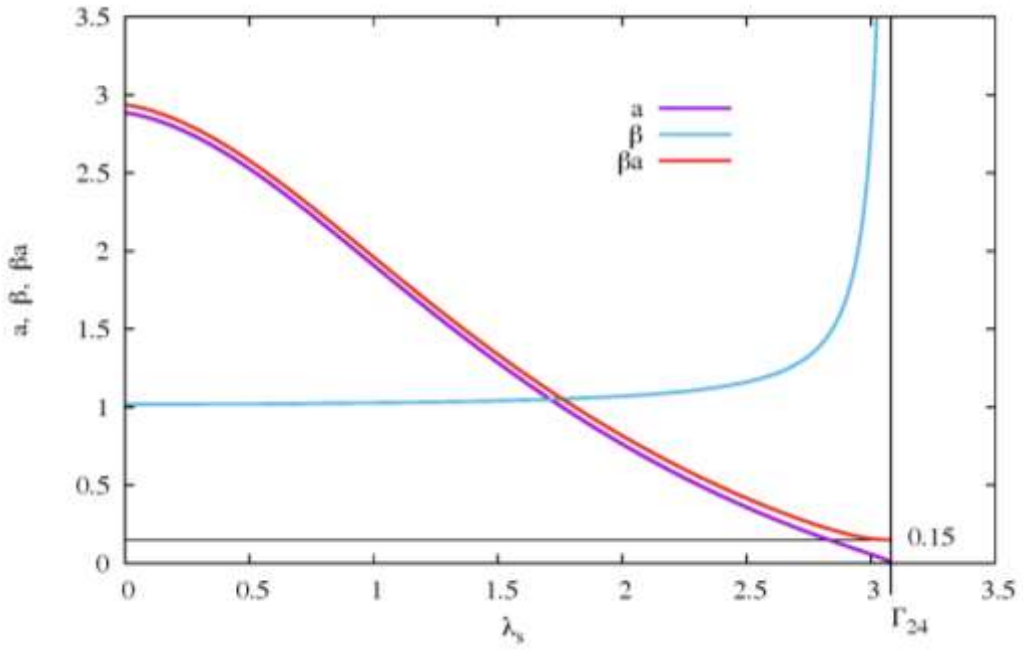

Figure 6. Values of a, β, βa with variable λ_s at constant μ = 4 and with αH_1^* = 0.1.

Additional iterations done by the Muller-Frank method are required in the next section for determining μ values given onshore head and distance values, as defined by Eqs. (30) and (31).

Fig. 7 is included to show the effects of zone changes as αH_1^* is increased. Contour plots analogous to Figs. 5a, 5b and 5c show the same general patterns, but compressed in accordance with the increasing compression of zones as shown in Fig. 7.

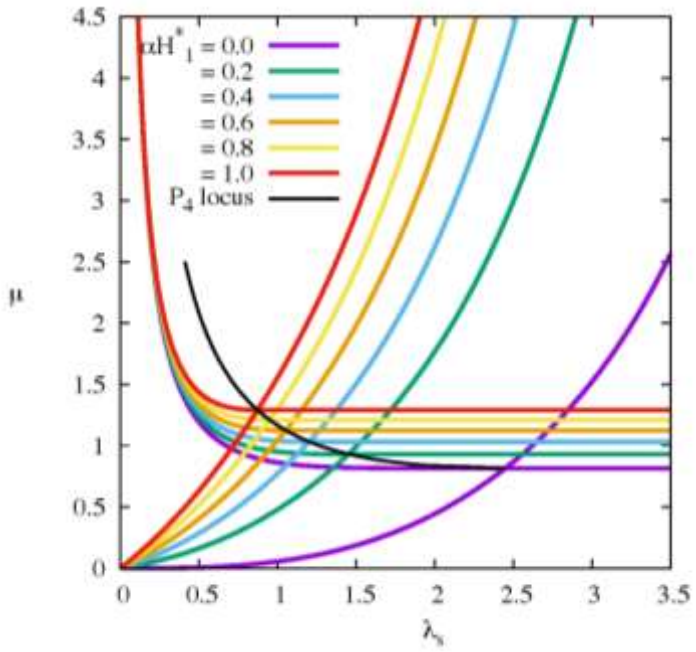

Figure 7. Zonal variations for $\alpha H_1^* = 0.0, 0.2, 0.4, 0.6, 0.8, 1.0$

4. Comparison with results from SEAWAT

An important requirement is to compare the sharp-interface analytical solutions with results from a more realistic model, such as SEAWAT. A limited comparison is made by taking the SEAWAT parameters and results from six models examined by Solórzano-Rivas and Werner (2017). The parameter values are H_s = 20 m, H_1 = 1 m, H = 10 m ($H_1^* = 0.1$), K = 10 m/d, $L_s(1)$ = 20 m, $L_s(2)$ = 3,000 m, K_v = {5, 1, 0.5, 0.01, 0.001, 0.0001} m/d corresponding to the six models designated {M_1, M_2, M_3, M_4, M_5, M_6}, and v_s = 0.025. μ and Q_0 are determined from inland head Eqs. (30) or (31), with h = 1 m relative to sea level, and inland distances $|x(1)|$ = 100 m and $|x(2)|$ = 490 m. Table 2 shows comparisons between SEAWAT, aquitard with freshwater, $\alpha = 1$, $\alpha H_1^* = 0.1$, designated 'fresh', and Bakker's results for $\alpha = 0$, $\alpha H_1^* = 0$. The meaning of Table 2 designations, such as 3(1), is model M_3 with $L_s(1)$, $x(1)$ and K_v value of 0.5 m/d.

Similarly, 6(2) is model M_6 with $L_s(2)$, $x(2)$ and K_v value of 0.0001 m/d. The (λ_s, μ) coordinates shown in Fig. 4 of the six models, in sequence M_1 to M_6, are: (0.373, 0.062); (0.622, 0.137); (0.756, 0.190); (0.916, 0.267); (1.484, 0.678); (1.963, 1.229). Figure 8 compares interface distributions from the three approaches for the model 4(2) (i.e., model M_4 with $L_s(2)$, $x(2)$ and K_v value of 1 m/d).

Table 2. Comparison of results from SEAWAT and analytical solutions for aquitards containing freshwater ("Fresh") or seawater ("Bakker").

Model	Method	Case	Q_0 (m^2/d)	Toe (m)	Tip (m)
1(1)	SEAWAT		0.3480	-33.1	1.8
	Fresh	1	0.3475	-35.3	1.7
	Bakker	1	0.3460	-35.0	4.6
2(1)	SEAWAT		0.3417	-31.9	6.4
	Fresh	1	0.3413	-34.1	6.2
	Bakker	1	0.3384	-33.6	13.5
3(1)	SEAWAT		0.3361	-30.9	10.9
	Fresh	1	0.3359	-33.0	10.7
	Bakker	3	0.3322	-32.3	20.0
4(2)	SEAWAT		0.0675	-129	95.0
	Fresh	1	0.0667	-153	91.6
	Bakker	1	0.0658	-148	168
5(2)	SEAWAT		0.0540	-43.9	472
	Fresh	1	0.0536	-70.2	469
	Bakker	1	0.0522	-59.0	722
6(2)	SEAWAT		0.0308	317	1958
	Fresh	2	0.0307	285	1963
	Bakker	2	0.0296	321	2771

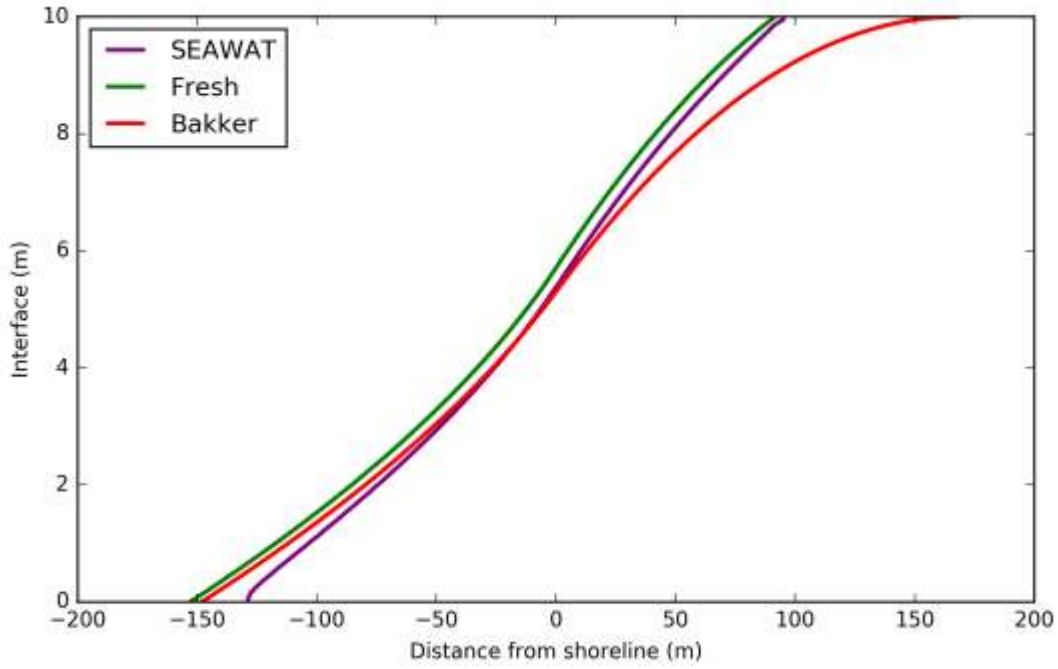

Figure 8. Interface between freshwater and seawater from SEAWAT (50% isochlor) and sharp-interface models (either freshwater ("Fresh") or saltwater ("Bakker") in the aquitard). The results correspond to model 4(2).

The results in Table 2 show that for all six models the assumption of freshwater in the aquitard outperforms the assumption of seawater, by comparison to SEAWAT's estimates, for the seaward discharge (Q_0) and the location of the tip. The average Q_0 discrepancy (analytical versus SEAWAT estimates) improves from 2% to 0.4% when the aquitard is presumed to contain freshwater instead of seawater. The higher Q_0 obtained when freshwater is used for the aquitard salinity is the intuitive outcome of the lower head (and therefore reduced resistance) of the subsea boundary when the water density in the aquitard is lower.

A marked improvement is obtained in the tip location, for which the average discrepancy reduces from 87% to 2% when freshwater rather than seawater is presumed for the

aquitard salinity. In the case of the seawater assumption, the more seaward tip location obtained using Bakker's (2006) seawater assumption is again caused by the higher head of the subsea boundary relative to the freshwater case, which requires a smaller outflow face.

The average discrepancy in the analytically derived toe location increases from 11% to 14% when the aquitard is presumed to contain freshwater instead of seawater, in contradiction to the tip and Q_0 findings. Both the 'Fresh' and 'Bakker' analytical toe locations are landward of the SEAWAT toe location, with the freshwater model landward of the Bakker model. The latter trend is caused by the lower head in the aquitard in the fresh model, which leads to higher flow rates for a given inland boundary head, and therefore greater head losses (by Darcy's Law) and more landward toe positions. Added to this effect, dispersion is known to produce toe locations that are seaward of estimates obtained from sharp-interface methods (e.g., Mehdizadeh et al., 2014). Werner (2017) applied SEAWAT to seawater intrusion problems with dispersion parameters set to zero, in a similar manner to the current methodology, and found analytical-numerical discrepancies consistent with those encountered here, and that could be explained by minor levels of artificial dispersion in SEAWAT. We expect, similarly, that artificial numerical dispersion in the SEAWAT predictions have produced toe locations that are seaward of sharp-interface values. Further investigation is needed to determine the impact of artificial dispersion on toe values produced by SEAWAT to ascertain whether the freshwater or seawater (in the aquitard) assumption best reproduces the correct toe locations. Regardless, on balance of the results, the improvements in both Q_0 and the tip location, from presuming that aquitard contains freshwater, more than offset the reduced accuracy in the toe location.

5. Concluding remarks

Previous analytical models of the extent of freshwater in offshore coastal aquifers have presumed that the overlying aquitard contains entirely seawater. However, this assumption has been challenged in a recent numerical modelling analysis, which concludes that revised analytical solutions are needed that accommodate alternative salinities in the offshore aquitard. In response, the current study presents a revised analytical formulation for the extent of offshore fresh groundwater by including the offshore aquitard salinity as an input variable, potentially ranging from freshwater to seawater. Otherwise, the same assumptions as previous formulations apply; namely the Dupuit approximation, steady-state conditions, homogeneity, and geometric uniformity.

Comparison of the new solution against numerical modelling confirms that the assumption of freshwater in the offshore aquitard outperforms the earlier seawater assumption, as suggested by Solórzano-Rivas and Werner (2017). In particular, the interface tip is well matched to the numerical results, compared to tip location errors of >100% when the aquitard is presumed to contain seawater. The freshwater assumption also produces slightly better estimates of freshwater discharge to the sea. Analytical values for the interface toe are landward of numerically derived estimates regardless of the presumed salinity in the aquitard. The fresh aquitard conditions produces slightly worse matches to numerical modelling relative to the assumption of seawater in the aquitard, although the effects of artificial dispersion in numerical estimates is expected to play a role in this comparison. Further work is needed to account for artificial dispersion in assessing the accuracy of analytically derived toe values.

Application of the proposed methodology requires consideration of coastline geomorphology, because in many cases, paleo-freshwater may occur in offshore aquifers, emplaced during historic glacial maxima. Offshore freshwater extents obtained with the current method neglect these sources of freshwater. An extension to the current method might include the evaluation of sea-floor sediment stability, whereby tidal fluctuations combined with vertical groundwater fluxes impact accretion/erosion rates.

Acknowledgements

We appreciate the provision of SEAWAT modelling results by Cristina Solórzano-Rivas. Adrian Werner is the recipient of an Australian Research Council Future Fellowship (project number FT150100403). The suggestions of three anonymous reviewers are gratefully acknowledged.

References

Bakker, M. (2006). Analytical solutions for interface flow in combined confined and semi-confined, coastal aquifers. *Adv. Water Resour*., 29(3), 417-425, doi: 10.1016/j.advwatres.2005.05.009.

Bakker, M., Miller, A.D., Morgan, L. and Werner, A.D. (2017). Evaluation of analytical solutions for steady interface flow where the aquifer extends below the sea. *J. Hydrol*., 551, 660-664, doi: 10.1016/j.jhydrol.2017.04.009.

Bear, J. (1979). *Hydraulics of Groundwater*. Dover, New York.

Byrd, P.F. and Friedman, M.D. (1971). *Handbook of Elliptic Integrals for Engineers and Scientists.* 2nd Edn, Springer-Verlag, Berlin.

Carlson, B.C. and Notis, E.M. (1981). Algorithm 577. Algorithms for incomplete elliptic integrals. *ACM Trans. Math. Software (TOMS)*, 7(3), 398-403.

Cohen, D., Person, M., Wang, P., Gable, C.W., Hutchinson, D., Marksamer, A., Dugan, B., Kooi, H., Groen, K., Lizarralde, D., Evans, R.L., Day-Lewis, F.D. and Lane Jr, J.W. (2010). Origin and extent of fresh paleowaters on the Atlantic continental shelf, USA. *Ground Water*, 48(1), 143-158, doi: 10.1111/j.1745-6584.2009.00627.x.

Edelman, J.H. (1972). Groundwater hydraulics of extensive aquifers. *International Institute for Land Reclamation and Drainage Bulletin, vol. 13*. Wageningen, The Netherlands (216 pp.).

Frank, W.L. (1958). Finding zeros of arbitrary functions. *J. Assoc. Comput. Mach.,* 5(2), 154-160.

Kooi, H., and Groen, J. (2001). Offshore continuation of coastal groundwater systems; predictions using sharp-interface approximations and variable-density flow modelling. *J. Hydrol*., 246(1-4), 19-35, doi: 10.1016/S0022-1694(01)00354-7.

Langevin, C.D., Thorne Jr., D.T., Dausman, A.M., Sukop, M.C. and Guo, W. (2008). SEAWAT version 4: a computer program for simulation of multi-species solute and heat transport: *U.S. Geological Survey Techniques and Methods*, Book 6, Chap. A22, 39 pp., Reston, Virginia.

Mathews, J.H. and Fink, K.D. (2004). *Numerical methods using Matlab*. 4th edn, Prentice-Hall, Upper Saddle River, New Jersey.

Mehdizadeh, S.S., Werner, A.D., Vafaie, F., Badaruddin, S. (2014) Vertical leakage in sharp-interface seawater intrusion models of layered coastal aquifers. *J. Hydrol.*, 519, 1097-1107, doi: 10.1016/j.jhydrol.2014.08.027.

Muller, D.E. (1956). A method for solving algebraic equations using an automatic computer. *Math. Tables Aids Comput.* 10, 208-15.

Post, V.E., Groen, J., Kooi, H., Person, M., Ge, S. and Edmunds, W.M. (2013). Offshore fresh groundwater reserves as a global phenomenon. *Nature*, 504(7478), 71-78, doi: 10.1038/nature12858.

Sikkema, P.C. and van Dam, J.C. (1982). Analytical formulas for the shape of the interface in a semi-confined aquifer. *J. Hydrol.*, 56(3-4), 201-220.

Solórzano-Rivas, S.C. and Werner, A.D. (2017). On modelling methods for estimating offshore groundwater. *Adv. Water Resour*. (In press), doi: 10.1016/j.advwatres.2017.11.025.

Werner, A.D. (2017). On the classification of seawater intrusion. *J. Hydrol.*, 551, 619-631, doi: 10.1016/j.jhydrol.2016.12.012.

Appendix A. Mathematical Analysis

Cases I and II

At the tip, $\xi_{1,2} = \lambda$, boundary conditions are

$$\phi = 0 \text{ and } \gamma_u = 0 \qquad \text{(A1)}$$

From Eq. (18), $\gamma_u = 0$ requires

$$a = 0 \qquad \text{(A2)}$$

Return to Eq. (19), and evaluate the indefinite integral with $a = 0$ as

$$\int \frac{\phi}{\sqrt{\phi^3 + 3/2\,\alpha H_1^* \phi^2}}\, d\phi = 2\sqrt{\phi + 3/2\,\alpha H_1^*} \qquad \text{(A3)}$$

Then

$$\xi_{1,2} = -\sqrt{6\phi + 9\alpha H_1^*} + b \qquad \text{(A4)}$$

From Eq. (19),

$$b = \lambda + 3\sqrt{\alpha H_1^*} \qquad \text{(A5)}$$

so that

$$\xi_{1,2} = -\sqrt{6\phi + 9\alpha H_1^*} + 3\sqrt{\alpha H_1^*} + \lambda \qquad \text{(A6)}$$

and from this

$$\phi = \frac{1}{6}\left[\left(\xi_{1,2} - \lambda\right)\left(\xi_{1,2} - \lambda - 6\sqrt{\alpha H_1^*}\right)\right], \quad 0 \le \xi_{1,2} \le \lambda \qquad \text{(A7)}$$

For all $\phi \neq 0$, Eq. (18) gives

$$\gamma_u = \sqrt{2/3\phi^3 + \alpha H_1^* \phi^2} \qquad \text{(A8)}$$

In the transition between Cases I and II, with the toe at the shoreline,

$$\xi_{1,2} = 0,\ \phi = 1,\ \gamma_u = \mu_t \qquad \text{(A9)}$$

Eq. (A8) then provides

$$\mu_t = \sqrt{2/3 + \alpha H_1^*} \qquad \text{(A10)}$$

Case I

At the shoreline, $\xi_1 = 0$, $\phi = \phi_0$ and $\gamma_u = \mu$, then Eq. (A8) gives

$$\phi_0^3 + 3/2\,\alpha H_1^* \phi_0^2 - 3/2\,\mu^2 = 0 \qquad \text{(A11)}$$

a cubic equation in ϕ_0, given αH_1^* and μ, and providing one real root and two complex conjugate roots. Eq. (A6) then gives an expression for λ:

$$\lambda = \sqrt{6\phi_0 + 9\alpha H_1^*} - 3\sqrt{\alpha H_1^*} \qquad \text{(A12)}$$

For onshore confined flow, with $q_z = 0$, Eqs. (9) and (13) reduce to

$$\frac{d}{d\xi_{1,2}}\left(\phi \frac{d\phi}{d\xi_{1,2}}\right) = 0 \qquad \text{(A13)}$$

which integrates to

$$\phi^2 = -2\mu\xi_{1,2} + \phi_0^2\ , \qquad -\delta \leq \xi_{1,2} \leq 0 \qquad \text{(A14)}$$

Distance δ from interface to toe where $\phi = 1$ and $\xi_{1,2} = -\delta$ is determined from Eq. (A14) as

$$\delta = \frac{1-\phi_0^2}{2\mu} \qquad \text{(A15)}$$

Case II

At the toe, $\xi_2 = 0$ and $\phi = 1$, then Eq. (A6) is also an expression for λ as

$$\lambda = \sqrt{6+9\alpha H_1^*} - 3\sqrt{\alpha H_1^*} \qquad \text{(A16)}$$

To find an expression for δ, the required differential equation is

$$\frac{d^2(KHh)}{dx^2} = \frac{\left(h - h_s + \alpha H_1^* v_s\right)}{c} \qquad \text{(A17)}$$

or in dimensionless variables

$$\frac{d^2\phi}{d\xi_2^2} = \phi + \alpha H_1^* \qquad \text{(A18)}$$

The general solution of this equation is

$$\phi = Ae^{\xi_2} + Be^{-\xi_2} - \alpha H_1^* \qquad \text{(A19)}$$

Boundary conditions are (i) $\xi = 0$, $\phi = 1$ and (ii) $\xi_2 = 0$, $-d\phi/d\xi_2 = \gamma_0 = \sqrt{2/3 + \alpha H_1^*}$.

These determine *A* and *B* so that

$$\phi = \frac{1}{2}\left(1 - \gamma_0 + \alpha H_1^*\right)e^{\xi_2} + \frac{1}{2}\left(1 + \gamma_0 + \alpha H_1^*\right)e^{-\xi_2} - \alpha H_1^*, \quad -\delta \le \xi_2 \le 0 \qquad \text{(A20)}$$

With $d\phi/d\xi_2 = -\mu$ at $\xi_2 = -\delta$, an expression for determining δ then follows, as

$$\frac{1}{2}\left(1+\gamma_0+\alpha H_1^*\right)e^{2\delta} - \mu e^{\delta} - \frac{1}{2}\left(1-\gamma_0+\alpha H_1^*\right) = 0 \qquad \text{(A21)}$$

which solves as

$$\delta = \log\left[\frac{\mu + \sqrt{\mu^2 + \left(1-\gamma_0+\alpha H_1^*\right)\left(1+\gamma_0+\alpha H_1^*\right)}}{\left(1+\gamma_0+\alpha H_1^*\right)}\right] \qquad \text{(A22)}$$

With $\xi_2 = -\delta$, Eq. (A20) gives

$$\phi_0 = \frac{1}{2}\left(1-\gamma_0+\alpha H_1^*\right)e^{-\delta} + \frac{1}{2}\left(1+\gamma_0+\alpha H_1^*\right)e^{\delta} - \alpha H_1^* \qquad \text{(A23)}$$

Cases III and IV

These cases have $\alpha \neq 0$. At the seaward end of the aquitard

$$\xi_{3,4} = \lambda_s, \ \phi = \qquad \text{(A24)}$$

Returning to Eq. (19), the integration is now made explicit in the form

$$\xi_{3,4} = -\sqrt{\frac{3}{2}}\int_{y_0}^{\phi} \frac{y}{\sqrt{y^3 + 3/2\,\alpha H_1^* y^2 + \alpha^3}}\,dy + const \qquad \text{(A25)}$$

The lower limit, y_0, can be changed at will, different values being absorbed into *const.* However, the square root of the cubic in the denominator suggests the use of standard expressions for elliptic integrals. This is achieved by first noting that the cubic can be factored as

$$y^3 + 3/2\,\alpha H_1^* y^2 + a^3 = \left(y+p\right)\left(y^2 - \left(a^3/p^2\right)y + a^3/p\right) \qquad \text{(A26)}$$

where p is real and the zeros of the quadratic in y are complex conjugates. If y_0 is replaced by $(-p)$, there is change of variable, $y = -pt$ and introduction of parameter $\beta = p/a$, then

$$\xi_{3,4} = \sqrt{\frac{3\beta a}{2}} \int_{-\phi/\beta a}^{1} \frac{t}{\sqrt{(1-t)\left(t^2 + (t+1)/\beta^3\right)}} dt + b \qquad \text{(A27)}$$

b is a constant to be determined by boundary conditions. The integral is now in standard form for evaluation in terms of elliptic integrals. Using Eqns. (243.07) and (341.53) of Byrd and Friedman (1971),

$$f(\phi, a, \beta) = \int_{-\phi/\beta a}^{1} \frac{t}{\sqrt{(1-t)\left(t^2 + (t+1)/\beta^3\right)}} dt$$

$$= \left(\frac{1}{\sqrt{g}} - \sqrt{g}\right) F(\theta, \kappa) + 2\sqrt{g} E(\theta, \kappa) - 2\sqrt{g} \frac{\sin\theta \sqrt{1 - \kappa^2 \sin^2\theta}}{1 + \cos\theta} \qquad \text{(A28)}$$

where $F(\theta, \kappa)$ and $E(\theta, \kappa)$ are incomplete elliptic integrals of the first and second kinds, respectively, with normal ranges $0 \le \theta \le \pi/2$ and $0 \le \kappa \le 1$. In this particular mathematical model, θ may lie in the range $\pi/2 < \theta < \pi$ for which the elliptic integrals are expressed as $F(\theta, \kappa) = 2K(\kappa) - F(\pi - \theta, \kappa)$ and $E(\theta, \kappa) = 2E(\kappa) - E(\pi - \theta, \kappa)$, where $K(\kappa)$ and $E(\kappa)$ are respective complete elliptic integrals of the first and second kinds (e.g., Byrd and Friedman, 1971). The other quantities in Eq. (A28) are defined by

$$g = \sqrt{1 + 2/\beta^3}, \quad \kappa = \sqrt{\left(1 + 1/(2\beta^3) + g\right)/(2g)}, \quad \theta = \cos^{-1}\left[\frac{g - 1 - \phi/(\beta a)}{g + 1 + \phi/(\beta a)}\right] \qquad \text{(A29)}$$

$\xi_{3,4}$ is now expressed in the compact form, for $0 \le \xi_{3,4} \le \lambda_s$,

$$\xi_{3,4} = \sqrt{\frac{3\beta a}{2}} f(\phi, a, \beta) + b \qquad \text{(A30)}$$

and b is obtained from Eq. (A30) as

$$b = \lambda_s - \sqrt{\frac{3\beta a}{2}} f(0, a, \beta) \qquad \text{(A31)}$$

When $\alpha = 0$ then $\beta = 1$ and all of the expressions above for $\xi_{3,4}$ and $f(\phi, a, \beta)$ reduce to those of Bakker (2006).

An important requirement is to determine the transition between Cases III and IV when the toe for each case coincides where $\xi_{3,4} = 0$, $\phi = 1$, and a, μ and λ_s are designated a_t, μ_t and λ_{st}, respectively. The non-linear equation for determining a_t follows from Eqs. (A30) and (A31) as

$$\sqrt{\frac{3\beta a}{2}} \left[f(1, a_t, \beta) - f(0, a_t, \beta) \right] + \lambda_{st} = 0 \qquad \text{(A32)}$$

Using the relationship between a_t and μ_t given by Eq. (A8), with $\gamma_u = \mu_t$ as Eq. (A10):

$$\mu_t = \sqrt{2/3\left(1 + a_t^3\right) + \alpha H_1^*} \quad \text{i.e.} \quad a_t = \left[3/2 \left(\mu_t^2 - \alpha H_1^* \right) - 1 \right]^{1/3} \qquad \text{(A33)}$$

which means that given λ_{st} then μ_t is found followed by a_t or vice versa.

Case III

Constant a is determined from the shoreline condition where $\gamma_0 = \mu$, $\phi = \phi_0$ and from Eq. (18), ϕ_0 is determined from the real root of the cubic equation

$$\phi_0^3 + 3/2\, \alpha H_1^* \phi_0^2 + a^3 - 3/2\, \mu^2 = 0 \qquad \text{(A34)}$$

together with

$$\sqrt{\frac{3\beta a}{2}}\left[f\left(\phi_0, a, \beta\right) - f\left(0, a, \beta\right)\right] + \lambda_s = 0 \qquad \text{(A35)}$$

Having found a, ϕ_0 is then calculated from Eq. (A34). The remaining quantity δ is then found from Eq. (34) of Case I, but with this new ϕ_0:

$$\delta = \frac{1-\phi_0^2}{2\mu} \qquad \text{(A36)}$$

For shoreline to toe, Eq. (A7) also holds:

$$\phi^2 = -2\mu\xi_3 + \phi_0^2, \qquad -\delta \le \xi_3 \le 0 \qquad \text{(A36)}$$

Case IV

The differential equation defining ϕ is the same as Eq. (A18) of Case II:

$$\frac{d^2\phi}{d\xi_4^2} = \phi + \alpha H_1^* \qquad \text{(A37)}$$

with boundary conditions,

$$\xi_4 = 0,\ \phi = 1$$

$$\xi_4 = -d/\lambda,\ \ d\phi/d\xi_4 = -\mu \qquad \text{(A38)}$$

providing the solution

$$\phi = \left(1 + \alpha H_1^*\right)\frac{\cosh\left(\delta + \xi_4\right)}{\cosh\delta} - \mu\frac{\sinh\xi_4}{\cosh\delta} - \alpha H_1^*, \quad -\delta \le \xi_4 \le 0 \qquad \text{(A39)}$$

It is now required to find δ. This is achieved by first determining an equation for a using two expressions for $\gamma = -\phi\, d\phi/d\xi_4$ from Eqs. (16) and (18), and the derivative of Eq. (A39), at $\phi = 1$:

$$\sqrt{2/3\left(1+a^3\right)+\alpha H_1^*} = -\left(1+\alpha H_1^*\right)\tanh\delta + \frac{\mu}{\cosh\delta} \qquad \text{(A40)}$$

Solving for 'a' and noting that $\lambda = \lambda_s - \delta$, then substituting in

$$\sqrt{\frac{3\beta a}{2}}\left[f\left(1,a,\beta\right) - f\left(0,a,\beta\right)\right] + \lambda_s - \delta = 0 \qquad \text{(A41)}$$

provides a non-linear equation for δ.

An expression for ϕ_0 now follows from Eq. (A39) with $\xi_4 = -\delta$:

$$\phi_0 = \frac{\left(1+\alpha H_1^*\right)}{\cosh\delta} + \mu\tanh\delta - \alpha H_1^* \qquad \text{(A42)}$$

Notation (respective equation numbers given in brackets)

α	Presumed salinity of the offshore aquitard (0 is seawater, 1 is freshwater)
β	Cubic equation factor (24), (A27)
δ	Dimensionless distance from the shoreline to the interface toe
ϕ	Dimensionless freshwater head above sea level (12)
ϕ_0	Shoreline value of ϕ
κ	Modulus of elliptic integrals (26)
λ	Dimensionless horizontal length to the interface tip
λ_s	Dimensionless horizontal length of the offshore aquitard (17)
γ_0	Shoreline value of γ_u (17)
γ_u	Dimensionless discharge (16)
η	Vertical thickness of freshwater in the offshore aquifer (7)
μ	Dimensionless discharge (17)

θ	Modular angle of elliptic integrals (26)
ρ_f	Freshwater density
ρ_s	Seawater density
ξ	Dimensionless horizontal distance (12)
$\xi_1, \ldots, \xi_4$	ξ for Cases I, II, III and IV – see Figure 3 for respective origins.
ζ	Dimensionless vertical distance from the aquifer base to the interface (12)
$\Gamma_{12}, \ldots, \Gamma_{34}$	Boundary values of μ versus λ_s, distinguishing Cases I to IV
a	Integration constant (15)
A	Coefficient of differential equation solution (A19)
b	Integration constant (19)
B	Coefficient of differential equation solution (A19)
c	H_1/k_v (10)
d	Distance from toe to shoreline
$E(\kappa)$	Complete elliptic integral of the second kind
$E(\theta,\kappa)$	Incomplete elliptic integral of the second kind (25)
$f(\phi,a,\beta)$	A function (25)
$F(\theta,\kappa)$	Incomplete elliptic integral of the first kind (25)
F_3, F_4	Two reference points (Cases III and IV) of coordinates (μ, λ_s)
g	An intermediate variable (26)
h	Head of the freshwater region within the offshore aquifer (3)
h_l	Freshwater head of a column of seawater above the top of the aquitard (1)
h_s	Freshwater head of a column of seawater above the top of the aquifer (5)
H	Thickness of the offshore aquifer (12)
H_1	Thickness of the offshore aquitard (3)
H_s	Depth of seawater above the offshore aquitard (1)

H_1^*	Dimensionless aquitard thickness (13)
K	Aquifer hydraulic conductivity
K_v	Vertical hydraulic conductivity of the offshore aquitard
$K(\kappa)$	Complete elliptic integral of the first kind
l_f	Leakage factor (12)
L	Horizontal distance from the origin to the interface tip
L_s	Offshore aquitard horizontal length
$M_1, \ldots, M_6$	Six reference points of coordinates (μ, λ_s), along boundaries
p	Root of cubic equation (24)
P_4	Reference point of coordinates (μ, λ_s), at the intersection of Cases I to IV
q_z	Vertical component of specific discharge through the offshore aquitard (3)
Q_0	Shoreline value of Q_x (17)
Q_x	Vertically integrated fresh groundwater discharge (8)
t	Integration variable (25)
t (subscript)	Subscript to indicate a parameter at the transition between Cases
v_s	Dimensionless seawater-freshwater density difference (2)
x	Horizontal spatial coordinate
y	Variable in a cubic form (24)
y_0	Lower integration limit (A25)
z	Vertical spatial coordinate
z_s	Elevation of the sea